An improved whitecap timescale for sea spray aerosol production flux modeling using the discrete whitecap method

ARTICLE · SEPTEMBER 2013

DOI: 10.1002/jgrd.50768

1 AUTHOR:

Adrian Callaghan
University of California, San Diego
19 PUBLICATIONS **174** CITATIONS

SEE PROFILE

An improved whitecap timescale for sea spray aerosol production flux modeling using the discrete whitecap method

Adrian H. Callaghan [1,2]

Received 5 February 2013; revised 14 August 2013; accepted 16 August 2013.

[1] The discrete whitecap method (DWM) to model the sea spray aerosol (SSA) production flux explicitly requires a whitecap timescale, which up to now has only considered a whitecap decay timescale, τ_{decay}. A reevaluation of the DWM suggests that the whitecap timescale should account for the total whitecap lifetime (τ_{wcap}), which consists of both the formation timescale (τ_{form}) and the decay timescale (timescale definitions are given in the text). Here values of τ_{form} for 552 oceanic whitecaps measured at the Martha's Vineyard Coastal Observatory on the east coast of the USA are presented, and added to the corresponding values of τ_{decay} to form 552 whitecap timescales. For the majority of whitecaps, τ_{form} makes up about 20–25% of τ_{wcap}, but this can be as large as 70% depending on the value of τ_{decay}. Furthermore, an area-weighted mean whitecap timescale for use in the DWM (τ_{DWM}) is defined that encompasses the variable nature of individual whitecap lifetimes within a given time period, and is calculated to be 5.3 s for this entire data set. This value is combined with previously published whitecap coverage parameterizations and estimates of SSA particle production per whitecap area to form a size-resolved SSA production flux parameterization ($dF(r_{80})/d\log_{10}r_{80}$). This parameterization yields integrated sea-salt mass fluxes that are largely within the range of uncertainty of recent measurements over the size range $0.029\ \mu m < r_{80} < 0.580\ \mu m$. Physical factors controlling whitecap lifetime such as bubble plume lifetime and surfactant stabilization are discussed in the context of SSA production from whitecaps.

Citation: Callaghan, A. H. (2013), An improved whitecap timescale for sea spray aerosol production flux modeling using the discrete whitecap method, *J. Geophys. Res. Atmos.*, *118*, doi:10.1002/jgrd.50768.

1. Introduction

[2] Breaking gravity waves at the ocean-atmosphere interface form primary sea spray aerosol (SSA) particles through the production of film drops, jet drops, and spume drops. These SSA particles are entrained upward from the ocean surface into the atmosphere above where they can form cloud condensation nuclei, directly scatter electromagnetic radiation, and transfer heat, mass, and momentum between the ocean and atmosphere [*Lewis and Schwartz*, 2004; *O' Dowd and de Leeuw*, 2007; *de Leeuw et al*., 2011]. SSA particles are composed of both inorganic sea salt and organic material and have been found to be enriched in organic material in biologically productive seawater [*O'Dowd et al*., 2004; *de Leeuw et al*., 2011]. Since roughly 70% of the Earth's surface is covered by oceans, accurate knowledge of the source function of SSA particles generated by breaking waves is a critical step in evaluating how SSA particles influence the Earth's climate [e.g., *Meskhidze et al*., 2013].

[3] Several methods exist for estimating the production flux of SSA particles from breaking waves and whitecaps, and the reader is referred to *Lewis and Schwartz* [2004] and *de Leeuw et al*. [2011] for comprehensive reviews. Here the focus is on the discrete whitecap method (DWM), which predicts the size-resolved interfacial flux of SSA particles ($dF(r_{80})/d\log r_{80}$) from the ocean surface to the atmosphere. Following *Monahan et al*. [1982], the DWM interfacial SSA flux can be written as

$$\frac{dF(r_{80})}{d\log_{10} r_{80}} = \frac{dE(r_{80})}{d\log_{10} r_{80}} \times \frac{W}{\tau_{decay}} \quad (1)$$

where $dE(r_{80})/d\log_{10}r_{80}$ is the number of SSA particles produced per unit logarithmic interval of particle radius at 80% relative humidity, (dr_{80}), during the decay of a unit area of whitecap (with units of number $\mu m^{-1}\,m^{-2}$), τ_{decay} is the e-folding timescale of the decaying whitecap area [e.g., *Monahan and Zietlow*, 1969], and W is the oceanic whitecap coverage (whitecap area per unit sea surface area), which is often parameterized in terms of wind speed at 10 m above the sea surface (U_{10}). The radius of an SSA particle, r, is a strong function of the relative humidity, and here it is evaluated at a relative humidity of 80% unless otherwise explicitly stated (the logarithm subscript 10 is dropped for

[1]School of Physics, Ryan Institute, National University of Ireland, Galway, Ireland.
[2]Now at Scripps Institution of Oceanography, University of California, San Diego, La Jolla, California, USA.

Corresponding author: A. Callaghan, Scripps Institution of Oceanography, University of California, San Diego, La Jolla, CA, USA. (callaghan.adrian@gmail.com)

2169-897X/13/10.1002/jgrd.50768

the remainder of the paper along with the use of r_{80} after dF and dE). Also, the convention of using logarithmic radius interval as presented in *de Leeuw et al*. [2011] is followed.

[4] The general whitecap method was first described by *Blanchard* [1963] who suggested that the global production of sea-salt nuclei (as SSA particles were then termed) could be obtained by multiplying the particle production rate per unit whitecap area by the global whitecap coverage. Subsequently, E. C. Monahan and colleagues [e.g., *Monahan et al*., 1982, 1986] pioneered the DWM as described by equation (1) above, as a means of predicting the size-resolved flux of SSA particles from the sea surface generated by air-entraining breaking waves. The DWM is "based on the contention that the number of sea spray droplets produced per unit area of sea surface per unit time is simply equal to the fraction of the sea surface over which whitecaps decay per unit time multiplied by the number of spray droplets produced during the decay of a unit area of whitecap" [*Monahan et al*., 1982].

[5] In developing the DWM, Monahan and colleagues performed laboratory experiments to measure the size-resolved number of SSA particles produced by a simulated breaking wave of maximum whitecap area A_o, (dE/dlogr_{80}) [e.g., *Monahan et al*., 1982, 1986]. These measurements included the aerosol particles produced by bursting bubbles during the entire lifetime of the visible whitecap foam (as detected by their photographic measurements). The measurements also included the aerosol particles produced after the visible whitecap had become practically undetectable with their optical measurement technique when smaller bubbles with radius, a, of order several hundred μm and less rose to the surface and burst. Therefore, the term dE/dlogr_{80} in equation (1), measured by Monahan and colleagues for a whitecap of maximum area $\approx 0.35\ \mathrm{m}^2$, represents the size-resolved number of SSA particles produced per unit whitecap area resulting from the complete degasing of the bubble plume formed from the air entrained by a breaking wave (assuming no loss of air due to dissolution).

[6] To extrapolate the laboratory findings to the open ocean to determine the rate of SSA particle production per unit ocean surface area, Monahan and colleagues combined dE/dlogr_{80} with W/τ_{decay}, where τ_{decay} was the e-folding decay time of the simulated whitecap in their laboratory experiments with a value of 3.53 s. A key assumption of the DWM was that under conditions of steady state whitecap coverage, the rate of decay of whitecap area per unit area sea surface would be equal to the rate of new whitecap area production per unit sea surface (E. C. Monahan, personal communication). As intended by Monahan and colleagues, the term W/τ_{decay} then represented the rate at which whitecap area was formed per unit sea surface area [see *Monahan* [1971, equations (2)–(5)]. The timescale, τ_{decay}, was not meant to characterize the time over which SSA particles were generated by the evolving whitecap and subsequent diffuse bubble plume. By combining dE/dlogr_{80} with W/τ_{decay}, *Monahan et al*. [1982, 1986] created the DWM which estimates the size-resolved rate of SSA particle production per unit sea surface area as a result of air-entraining breaking waves or whitecaps. The whitecap coverage parameterization used was that presented in *Monahan and O'Muircheartaigh* [1980]. The usefulness and effectiveness of this approach to model SSA production flux can be seen through the wide and routine use of the *Monahan et al*. [1986] DWM formulation and subsequent modified forms [e.g., *Gong*, 2003; *Jaeglé et al*., 2011] in global chemical transport models such as GLOMAP (http://researchpages.net/glomap/) and GEOS-Chem (http://geos-chem.org/) [e.g., *Spracklen et al*., 2005; *Korohonen et al*., 2010; *Gantt et al*., 2012].

[7] Several assumptions are central to the DWM as described above. These include that (i) the rate of whitecap area production per sea surface is equal to the rate of decay of whitecap area per sea surface area in conditions of steady state whitecap coverage, (ii) a single decay timescale is applicable to all whitecaps regardless of size, and (iii) the whitecap timescale should only consider the decay time of whitecaps. Additionally, the shape and magnitude of dE/dlogr_{80} used in the DWM is typically constant; however, it was recognized by *Monahan et al*. [1986] that it should be determined separately for weakly spilling and strongly plunging breaking waves. Previous laboratory and field studies have shown that an exponential function of time is a good model for the decay of whitecap area, but that these decay timescales are not constant and have been found to vary by up to a factor of 50 [e.g., *Monahan and Zietlow*, 1969; *Nolan*, 1988; *Sharkov*, 2007; *Callaghan et al*., 2012]. In addition, recent laboratory studies have explicitly demonstrated the importance of bubble plume characteristics and the presence of amphiphilic organic material (surfactants) in determining individual whitecap decay times [*Callaghan et al*., 2013].

[8] Here new oceanic measurements of the lifetime of 552 oceanic whitecaps are presented which include the formation timescale (τ_{form}) of the measured whitecap areas as well as the decay timescale (whitecap timescales are defined in section 2). The whitecap decay timescales have previously been reported in *Callaghan et al*., [2012]. These oceanic data show that (i) the increase in whitecap area is almost linear in time and often not equal in magnitude to the whitecap decay timescale, (ii) individual whitecap lifetime timescales vary by over a factor of 20, and (iii) area-weighted average whitecap lifetimes cannot be expected to be constant between different observational periods. Given these findings, a modified form of the whitecap timescale for use in the DWM is proposed. This timescale takes into account the entire whitecap lifetime (and not only the whitecap decay time) and also accounts for the variable nature of whitecap lifetimes. Section 2 provides a brief description of the wave breaking process, whitecap evolution, and time to first SSA production after air-entrainment. Section 3 defines the formation and decay timescales and sets forth the rationale for a revised DWM whitecap timescale. The study area and the image processing methodology are described in section 4. The whitecap formation timescale data are presented in section 5, and a revised DWM SSA production flux parameterization is presented. Section 6 discusses the physical processes that control the lifetime of individual whitecaps and how these processes may affect SSA production flux. Finally, conclusions and suggestions for future work are given in section 7.

2. Wave Breaking, Whitecap Evolution, and SSA Production

[9] The lifetime of a single whitecap may be broadly divided into three overlapping stages that encompass, (i) active

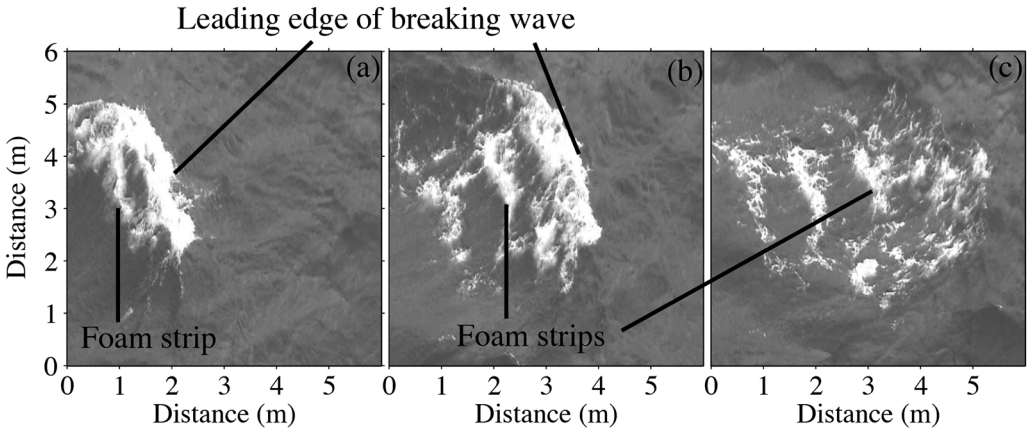

Figure 1. (a–c) Developing oceanic whitecap from the study site south of Martha's Vineyard. The wave is breaking from left to right and successive images are separated in time by 750 ms. The first image is from 1.2 s after the onset of breaking. The sequence of images shows the development of several distinct foam strips and isolated bubble plumes behind the leading edge of the breaking wave as a direct consequence of multiple air-entrainment events during active breaking.

air-entrainment, (ii) buoyant bubble rising, and (iii) thin film fluid drainage from, and rupture of, whitecap foam cells. When a sufficiently energetic surface gravity wave becomes unstable and breaks, air is entrained into the water column to a depth that is governed by the scale and slope of the breaking wave [*Lamarre and Melville*, 1991; *Callaghan et al*., 2013]. At least two mechanisms are responsible for air-entrainment: first, the overturning wave crest strikes the water surface below forming a reactionary splash-up, and second, a cavity is formed when the overturning crest reconnects with the water surface which then disintegrates as breaking develops [*Deane and Stokes*, 2002]. Both the splash-up and cavity collapse can form distinctive bubble plumes. During active air entrainment, a burst of noise is generated by bubble formation during what is termed the acoustically active phase and which has been measured to last about 1 s for laboratory generated breaking waves [*Deane and Stokes*, 2002]. These laboratory measurements indicate that bubbles begin to form within about 100 ms ($\tau_{bub,form}$) of the beginning of wave breaking [see, *Deane and Stokes*, 2002, Figure 3].

[10] Depending on the scale, slope, and energy dissipated by a breaking wave, multiple air entrainment events may occur within a single whitecap. Consequently, whitecaps are often composed of one or more foam strips and isolated bubble plumes. This can be seen in Figure 1 which displays three images showing the evolution of a breaking wave and resulting surface whitecap foam. Up to three distinctive foam strips along with other isolated bubble plumes are evident. The time between successive images is ~750 ms, the first image was taken ~1.2 s after breaking began, and the duration of breaking for this event was about 2.5 s. The occurrence of multiple foam strips and bubble plumes is directly related to staggered air-entrainment events during the wave breaking process. In Figure 1a, the first foam strip has already formed behind the leading edge of the breaking wave crest. As the whitecap area grows, the breaking wave crest continues to entrain air and forms the subsequent foam strips seen in the second and third panels. As a result of staggered air-entrainment during wave breaking, bubble plume evolution, whitecap decay, and commencement of SSA particle production associated with each of the foam strips can also be expected to be staggered in time throughout the whitecap formation phase.

[11] Following active air-entrainment, the whitecap enters the acoustically quiescent phase and the bubbles within the plume rise to the surface (also termed degassing) [*Deane and Stokes*, 2002]. Photographic observations from breaking waves in the surf zone suggest that bubbles of different sizes are randomly and homogenously distributed in plumes that are formed within the first second or so of breaking [*Deane*, 1997]. Since the rise speed of bubbles in water is a strong function of bubble size, bubble distributions begin to evolve rapidly with time after air entrainment. The terminal rise speed for a bubble of radius 1 mm is about 20 cm/s [e.g., *Fan and Tsuchiya*, 1990], so that the minimum time needed for a millimeter bubble with an initial depth of 1–2 diameters (2–4 mm) to rise to the surface (τ_{rise}) is about 10 to 20 ms. The turbulence generated by breaking waves can extend the time taken for bubbles to reach the surface so that the estimation of $\tau_{rise} \approx 10$–20 ms must be considered a lower bound and may be more appropriate for bubbles at the edge of a bubble plume.

[12] Once at the surface, the lifetime of the risen bubbles, or what we also refer to as whitecap foam or foam cells, is dictated by turbulent forces, gravity-driven thin film fluid drainage, gradients in surfactants giving rise to stabilizing Marangoni forces, and intermolecular forces which may act to further stabilize or destabilize the thin foam fluid films at thicknesses of ca. 50–100 nm [e.g., *Scheludko*, 1967; *Manev and Nguyen*, 2005; *Henry*, 2010]. In the absence of surfactants, the drainage to the point of rupture is expected to happen within milliseconds [*Henry*, 2010], and results from *Deane* [2013] suggest that this occurs after about 10–20 ms for millimeter size bubbles in clean tap water. However, surfactants are ubiquitous in the oceans [*Garrett*, 1967a] and will act to reduce thin film drainage rates, thereby extending the lifetime of bubbles in natural oceanic water. Laboratory data from *Modini et al*. [2013] using filtered natural seawater suggest that a lower bound for film drainage

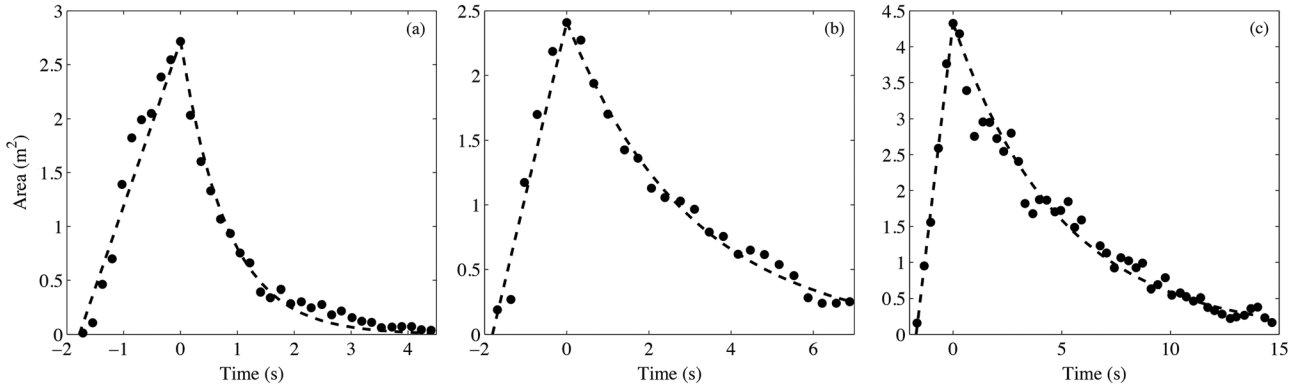

Figure 2. The evolution of whitecap area for three different breaking waves. The initial increase in area is nearly linear whereas the decrease is well approximated by an exponential decay. The values of τ_{form} and τ_{decay} are (a) 0.8 s and 0.9 s; (b) 0.9 s and 3.1 s; (c) 1 s and 5 s, respectively (see equation (2) and (3)). Note the different *y*-axis scales.

to the point of rupture ($\tau_{\mathrm{bub,drain}}$) for individual bubbles on a quiescent water surface, is about 200 ms for millimeter bubbles. It is important to note that given the turbulent nature of a breaking wave, it is likely that some bubbles rupture prematurely due to disruptive external forces before fluid drainage to the point of rupture can occur without interruption. Therefore, the minimum actual lifetime of a bubble on the sea surface within a breaking wave may be less than the estimate of 200 ms for $\tau_{\mathrm{bub,drain}}$.

[13] Taking values for $\tau_{\mathrm{bub,form}}$, $\tau_{\mathrm{bub,rise}}$, and $\tau_{\mathrm{bub,drain}}$ to be 100 ms, 10 ms, and 200 ms, respectively, we estimate that the minimum time needed for production of SSA particles to begin (τ_{SSA}) is of the order ~310 ms after the onset of wave breaking and bubble plume generation. Given that active wave breaking can last up to several seconds, SSA particles must be expected to be produced before active breaking is complete. Once active breaking is complete, SSA particle production may last for the order of tens of seconds which is typically longer than timescales associated with surface foam persistence [e.g., *Woolf et al*., 1987; *Bowyer et al*., 1990]. This can be attributed to the size-dependent rise speed of bubbles in water and also to the decaying turbulence which has a greater influence on retarding the rise of smaller, less buoyant bubbles [*Deane et al*., 2013]. Some fraction of these smaller bubbles of radius order several hundred μm and less may rise to the surface in isolation and burst on a relatively quiescent water surface [*Bowyer et al*., 1990]. As shown schematically in *Woolf et al*. [1987, Figure 4], this fractionation of the bubble population causes a distinct evolution in the rate of production of film drops and jet drops with time after wave breaking begins.

3. A New Timescale for the Discrete Whitecap Method, τ_{DWM}

[14] Before the DWM timescale (τ_{DWM}) is derived, the terms whitecap formation timescale and whitecap decay timescale as used here are explicitly defined. Figures 2a–2c show time series of the area of three evolving individual whitecaps, each with a distinct whitecap area growth or formation phase followed by a decay phase. The well-defined peak in the whitecap area time series allows the evolving whitecap area to be operationally separated into a formation phase and a decay phase. In reality, the peak in area marks the point when growth and decay processes are in equilibrium. To quantify the whitecap formation phase, the whitecap formation timescale (τ_{form}) is defined as

$$\tau_{\mathrm{form}} = \frac{1}{A_o}\int_{t=-\infty}^{t=0} A(t)\mathrm{d}t \tag{2}$$

where $A(t)$ is the evolving whitecap area, A_{o} is the maximum surface whitecap area reached at $t = 0$ s. The analytic form of the growth phase is approximated by performing a least-squares fit of a straight line to the measured whitecap area from $A(t) = 0$ to A_o. Since a straight line is used to approximate the nearly linear whitecap formation phase, the characteristic τ_{form} is equal to half the time taken for the whitecap area to reach A_o.

[15] Similarly, the decay timescale for an individual whitecap is defined as

$$\tau_{\mathrm{decay}} = \frac{1}{A_o}\int_{t=0}^{t=\infty} A(t)\mathrm{d}t \tag{3}$$

where $A(t)$ is approximated by the least-squares fitting of an exponential function of time to the decaying whitecap area. As seen from Figure 2, a simple exponential function of time adequately represented the temporal decay of these measured whitecap areas. *Callaghan et al*. [2012] do note that the decay of some whitecaps shows a departure from exponential decay, but that ensemble averages of multiple whitecaps are well characterized by exponential decay. Combining the result of equations (2) and (3) gives the whitecap timescale (τ_{wcap}) for an individual whitecap such that $\tau_{\mathrm{wcap}} = \tau_{\mathrm{form}} + \tau_{\mathrm{decay}}$.

[16] To determine the DWM whitecap timescale, we begin by rewriting equation (1) and replacing τ_{decay} with τ_{DWM} in equation (4) below

$$\frac{\mathrm{d}F}{\mathrm{d}\log r_{80}} = \frac{\mathrm{d}E}{\mathrm{d}\log r_{80}} \times \frac{W}{\tau_{\mathrm{DWM}}} \tag{4}$$

where τ_{DWM} is initially unknown. Consider a constant mean number of size-resolved SSA particles generated per unit sea surface area per unit time within some given observational time period of duration, T, and observational sea surface area, A_{obs},

from M distinct air-entraining breaking waves ($\mathrm{d}F/\mathrm{dlog}r_{80}$). The left-hand side of equation (4) can be rewritten as

$$\frac{\mathrm{d}F}{\mathrm{d}\log r_{80}} = \frac{\sum_{i=1}^{M}\Delta n_i(r_{80})}{A_{\mathrm{obs}}T} \tag{5}$$

where $\Delta n_{\mathrm{i}}(r_{80})$ is the size-resolved number of SSA particles produced by the ith air-entraining breaking wave out of a total of M breaking waves (henceforth, the terms air-entraining before wave breaking and r_{80} after Δn_i are dropped). A characteristic size-resolved number of SSA particles per breaking wave, $\Delta\tilde{n}(r_{80})$, can be chosen such that equation (5) can be rewritten as

$$\frac{\mathrm{d}F}{\mathrm{d}\log r_{80}} = \frac{M\Delta\tilde{n}}{A_{\mathrm{obs}}T} \tag{6}$$

where the term r_{80} is dropped after $\Delta\tilde{n}$. Focusing on the right-hand side of equation (4), the term $\mathrm{d}E/\mathrm{dlog}r_{80}$ may be rewritten as

$$\frac{\mathrm{d}E}{\mathrm{d}\log r_{80}} = \frac{\Delta\tilde{n}}{\tilde{A}_o} \tag{7}$$

where $\tilde{A}_o$ is a characteristic maximum whitecap area defined to be the mean maximum whitecap area ($\tilde{A}_o = \sum_{i=1}^{M}A_{o,i}/M$). As mentioned in the introduction, DWM formulations typically use a constant $\mathrm{d}E/\mathrm{dlog}r_{80}$ applicable to all whitecap areas at all wind speeds, although it is likely to vary with different breaking wave intensities [*Monahan et al.*, 1986]. For a given observational area and time period in steady state conditions, the whitecap coverage (W) can be rewritten as

$$W = \frac{\sum_{i=1}^{M}\int A_i(t)\mathrm{d}t}{A_{\mathrm{obs}}T} \tag{8}$$

where the integral is evaluated over the entire lifetime of each whitecap. Using equations (2) and (3), the time integral of evolving whitecap area can be rewritten as

$$\int A_i(t)\mathrm{d}t = A_{o,i}\left(\tau_{\mathrm{form},i} + \tau_{\mathrm{decay},i}\right) = A_{o,i}\tau_{\mathrm{wcap},i} \tag{9}$$

and when substituted into equation (8) yields

$$W = \frac{\sum_{i=1}^{M}A_{o,i}\tau_{\mathrm{wcap},i}}{A_{\mathrm{obs}}T} \tag{10}$$

The sum in equation (10) may be rewritten as the product of a characteristic or effective whitecap timescale, $\tau_{\mathrm{wcap,eff}}$, and M number of whitecaps with characteristic maximum whitecap area $\tilde{A}_o$, $\left(M\tilde{A}_o\tau_{\mathrm{wcap,eff}} = \sum_{i=1}^{M}A_{o,i}\tau_{\mathrm{wcap},i}\right)$. Thus, equation (10) is rewritten as

$$W = \frac{M\tilde{A}_o\tau_{\mathrm{wcap,eff}}}{A_{\mathrm{obs}}T} \tag{11}$$

where $\tau_{\mathrm{wcap,eff}}$ is explicitly defined as the area-weighted mean whitecap lifetime for M breaking waves or whitecaps in a given observational period as written in equation (12) below.

$$\tau_{\mathrm{wcap,eff}} = \frac{\sum_{i=1}^{M}A_{o,i}\tau_{\mathrm{wcap},i}}{M\tilde{A}_o} \tag{12}$$

[17] From equation (11), for a given sea surface area and observation period duration, steady state whitecap coverage is achieved when the wave breaking rate ($M/(A_{\mathrm{obs}}T)$), the characteristic maximum whitecap scale ($\tilde{A}_o$), and the effective whitecap lifetime ($\tau_{\mathrm{wcap,eff}}$) all remain constant, or their product remains constant. Equation (4) can now be rewritten in terms of its constituent components by substituting in equations (6), (7), and (11) to yield

$$\frac{M\Delta\tilde{n}}{A_{\mathrm{obs}}T} = \frac{\Delta\tilde{n}}{\tilde{A}_o} \times \frac{M\tilde{A}_o\tau_{\mathrm{wcap,eff}}}{A_{\mathrm{obs}}T} \times \frac{1}{\tau_{\mathrm{DWM}}} \tag{13}$$

[18] Rearranging equation (13) into equation (14) below shows that τ_{DWM} must be equal to the area-weighted mean whitecap lifetime as defined in equation (12).

$$\tau_{\mathrm{DWM}} = \left[\frac{M\Delta\tilde{n}}{A_{\mathrm{obs}}T}\right]^{-1} \times \frac{\Delta\tilde{n}}{\tilde{A}_o} \times \left[\frac{M\tilde{A}_o\tau_{\mathrm{wcap,eff}}}{A_{\mathrm{obs}}T}\right] = \tau_{\mathrm{wcap,eff}} \tag{14}$$

[19] The development of equations (4)–(14) indicates that the timescale in the original DWM (equation (1)) is incomplete as it does not take into account the formation timescale of whitecap area evolution. In the context of the DWM as originally described by *Monahan et al.* [1982], τ_{decay} in equation (1) should be replaced by τ_{DWM} as written in equation (4). Additionally, equation (13) highlights the importance of both the wave breaking rate and characteristic maximum whitecap area in determining the SSA production flux since τ_{DWM} must be equal to $\tau_{\mathrm{wcap,eff}}$ and as such, appears in both the numerator and the denominator. These implications are further discussed in section (6) below.

4. Study Area and Methods

[20] A detailed description of the study area, experimental details, and image processing procedure has been given in *Callaghan et al.* [2012], and a brief summary is given here. Sea surface images were taken with a 5 megapixel camera between 3 and 6 frames per second during the Surfaces Processes and Acoustics Communication Experiment in October 2008 (SPACE08). The camera was mounted on the Air Sea Interaction Tower (ASIT) located 3 km south of Martha's Vineyard on the east coast of the USA (the ASIT forms part of the Martha's Vineyard Coastal Observatory, MVCO). The data presented here are from four observation time periods (periods I–IV) characterized by different wind and wave conditions. These four periods were chosen because of the good image quality within each period (there was no contamination from sun glint or sky reflection), and to provide a relatively large range of wind speeds. Wind and wave data were obtained from the MVCO and these data are presented in *Callaghan et al.* [2012, Table 1 and Figure 1]. The mean, maximum, and minimum wind speeds along with the continuous length of each period are given here in Table 1. The wind speed was relatively steady for observation periods I–III, but period IV, which directly followed period III, was exceptional insofar as the wind speed rapidly increased from 6.8 m/s at the end of period III to 15.1 m/s over a 1 h period.

[21] The digital images were analyzed according to the threshold method of *Callaghan and White* [2009] to segment the image into whitecap and background water. The image

Table 1. The Calculated Values of the Effective Whitecap Timescales, Standard Deviation of Individual Whitecap Timescales, Wind Speed and Observation Period Duration for Each Individual Observation Period and for the Data Set as a Whole[a]

	Period I	Period II	Period III	Period IV	All Data
$\tau_{form,eff}$ (s)	1.0	1.0	0.8	0.9	1.0
$\tau_{decay,eff}$ (s)	4.5	4.9	1.4	3.1	4.3
τ_{DWM} (s)	5.5	5.9	2.2	4.1	5.3
$\sigma(\tau_{form})$	0.3	0.3	0.3	0.3	0.3
$\sigma(\tau_{decay})$	1.5	1.6	0.6	1.3	1.6
$\sigma(\tau_{wcap})$	1.6	1.8	0.7	1.5	1.8
U_{10} (m/s)	11.4	8.2	5.7	13.7	
$U_{10,max}$ (m/s)	12.5	9.5	6.8	15.1	
$U_{10,min}$ (m/s)	10.3	7.2	4.2	6.8	
T (h)	9	8	3	1	

[a]Rows 1–3 show values of the effective formation timescale ($\tau_{form,eff}$), effective decay timescale ($\tau_{decay,eff}$) and their sum, the effective whitecap timescale or equivalently the DWM whitecap timescale (τ_{DWM}), for each period and the entire data set. Rows 4–6 show the standard deviation (σ) of individual formation times, decay times, and whitecap lifetimes, respectively, for each period and for the entire data set. Also shown is the mean wind speed (U_{10}), maximum wind speed ($U_{10,max}$), and minimum wind speed ($U_{10,min}$) for each period and the duration of each period (T).

footprint dimensions and area were calculated following *Lippmann and Holman* [1989]. The nominal image footprint was 339 m^2 but varied by ± 5% depending on the tide, and the mean pixel area was of order 1 cm^2. The image processing routine accounts for the flocculence of the whitecap foam such that the outer bounding area completely containing each whitecap was always greater than the area of the whitecap foam within that area. A time series of the area evolution was calculated for each whitecap from first instance of visible air-entrainment until the decaying foam patch (i) decreased to an area less than 0.01 m^2, (ii) was partially advected out of the image, or (iii) was replenished by foam from another breaking wave. Only whitecaps with maximum areas greater than 0.2 m^2 were used in this analysis. Example whitecap area time series are shown in Figure 2, and they have been chosen to highlight the natural variability of individual whitecaps measured. There was some deviation from a perfect linear increase and exponential decrease in whitecap area with time, but overall, the whitecaps examined here were well-described by these simple functions and they always exhibited a distinct maximum area, A_o. As a result of the limited field of view of the camera, time series for the largest whitecaps (with estimated $A_o > 30$ to 40 m^2) could not be estimated because the breaking wave either did not completely finish breaking within the image footprint, or the resulting foam patch was partially or fully advected out of the field of view within 1–2 s after active breaking ceased.

5. Results

[22] As determined in section 3, τ_{DWM} is derived from knowledge of the area-weighted mean value of the sum of formation and decay times for all whitecaps in a given observational period. As stated above, the 552 individual whitecap decay times have been reported in *Callaghan et al*. [2012], and here we present the corresponding 552 whitecap formation timescales before proceeding to calculate τ_{DWM}.

5.1. Whitecap Formation Timescale, τ_{form}

[23] Distributions of individual values of τ_{form} for each of the four observation time periods comprising the entire 552 breaking wave data set, along with the distribution for the entire data set as a whole, are shown in Figure 3a. A Student's t test [*Middleton*, 2000] revealed that the mean values of τ_{form} were not statistically different across all four periods at the 99% confidence level, except for period I which was statistically different to period II and period III. The values of τ_{wcap} between all periods were determined to be statistically significantly different at the 95% confidence level using the same statistical test as above. For all values of τ_{form}, 90% ranged between 0.4 and 1.5 s, and each of the four time period distributions had distinctive peaks between 0.6 and 0.7 s. Given the almost linear increase in whitecap area and the integral definition of τ_{form}, the total breaking duration (τ_{brk}) is equal to twice the value of τ_{form}. The minimum τ_{brk} value for the entire data set is greater than 0.31 s, the τ_{SSA} estimated in section 2. Figure 2a implies that the duration of active wave breaking for the majority of the measured breaking waves was about 1 to 2 s.

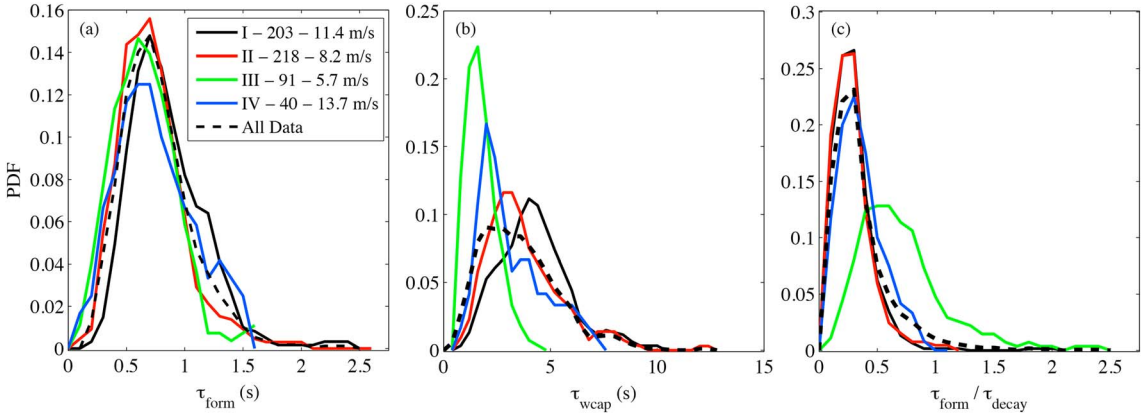

Figure 3. (a) The distribution of τ_{form} for the four observation periods in the study and the combined data set of 552 individual breaking wave events. The legend shows the number of processed whitecaps and the mean wind speed for each observation period. (b) The distribution of τ_{wcap} ($\tau_{form} + \tau_{decay}$) for observation periods and the entire data set. (c) The ratio of the formation to decay timescales for the four observation periods in the study and the combined data set.

[24] Distributions of whitecap lifetime ($\tau_{wcap} = \tau_{form} + \tau_{decay}$) are shown in Figure 3b for each time period and for the entire data set. As can be seen in Figure 3b, there is more variability in τ_{wcap} than in τ_{form}, which is primarily driven by the variability in τ_{decay}. The values of τ_{decay} presented in *Callaghan et al*. [2012] for individual whitecaps lie between 0.2 and 10.4 s and are consistent with previous oceanic values reported in *Nolan* [1988] and *Sharkov* [2007].

[25] To examine the relative magnitude of formation to decay timescales, and hence their respective contributions to the overall whitecap timescale, their ratio $\psi = \tau_{form} / \tau_{decay}$ is shown in Figure 3c for each individual period and for the entire data set. For three out of the four observation periods, ψ peaks around 0.2–0.3 while for period III when decay times were lowest, ψ had a broader distribution and a less-defined peak at about 0.5–0.6. The minimum and maximum values of ψ for the entire data set were 0.07 and 2.3, respectively. For the majority of the whitecaps, the formation phase comprised 20% to 25% of the total whitecap lifetime, but this was as large as 70% or more depending on the magnitude of the decay time. Given the relatively small variability of τ_{form} across the data set, its relative contribution to the overall whitecap timescale (τ_{wcap}) was primarily dependent on the magnitude of the whitecap decay time.

5.2. Estimate of τ_{DWM}

[26] The value of τ_{DWM} must be expected to vary from time period to time period and from location to location, depending on physical factors such as, but not limited to, the wave spectrum and its degree of development, wave age, wave breaking slope, wave breaking scale, wave-wave interaction, wave-current interaction, and surfactant concentration and composition. The value of τ_{DWM} can be broken down into contributions from the formation and decay phases of whitecap lifetime which we call $\tau_{form,eff}$ and $\tau_{decay,eff}$ and are simply the area-weighted mean formation and decay timescales, respectively. The calculated values of $\tau_{form,eff}$, $\tau_{decay,eff}$, and their sum τ_{DWM} are shown in Table 1, both for the individual observation periods and for the data set as a whole. Also shown for reference are the standard deviations of τ_{form}, τ_{decay}, and τ_{wcap} for each period and the entire 552 event data set. The values for τ_{DWM} differ from the laboratory determined decay time of *Monahan et al*. [1982], 3.53 s, by between −38% and +67%, which only encompasses the decay phase of a whitecap, and which is the whitecap timescale typically used in the DWM. There is a range of a factor of 2.7 in the values of τ_{DWM} across all time periods, which reduces to 1.4 when period III is excluded. As stated above, for this study, the limited camera field of view did not permit the decay time to be calculated for the largest whitecaps so that the values of $\tau_{decay,eff}$, and hence τ_{DWM}, reported in Table 1 are likely to be lower bounds.

5.3. Application of τ_{DWM} to SSA Production Flux

[27] The SSA production flux can be estimated using equation (4) above, where the value of the whitecap coverage is expected to completely determine the environmental forcing conditions. The vast majority of whitecap coverage parameterizations are functions of wind speed only [*Anguelova and Webster*, 2006], such that the SSA production flux from the discrete whitecap method is ultimately scaled with wind speed (U_{10}). To evaluate the SSA particle production flux, we use the $dE/d\log r_{80}$ expression from the Gong-Monahan model [*Gong*, 2003] as reported in *de Leeuw et al*., 2011, the whitecap coverage parameterizations of *Callaghan et al*. [2008a] (their equations (1) and (2) for wind speeds below and above 10.18 m/s respectively) and the value of τ_{DWM} for the entire data set from Table 1 (5.3 s). This leads to parameterizations for $dF/d\log r_{80}$ for two wind speed ranges which are written as

$$\frac{dF}{d\log r_{80}} = \frac{93.55}{\tau_{DWM}}(U_{10} - 3.7)^3 r_{80} \times \left(1 + 0.057 r_{80}^{3.45}\right) \bullet \exp\begin{pmatrix} 3.68 \times \exp\left[-5.33(0.433 - \log r_{80})^2\right] \\ -4.7 \ln r_{80}\left[1 + \Theta r_{80}\right]^{-0.017 r_{80}^{-1.44}} \end{pmatrix}, \quad (3.7 < U_{10}(m/s) \le 10.18), \tag{15a}$$

and

$$\frac{dF}{d\log r_{80}} = \frac{14.18}{\tau_{DWM}}(U_{10} + 1.98)^3 r_{80} \times \left(1 + 0.057 r_{80}^{3.45}\right) \bullet \exp\begin{pmatrix} 3.68 \times \exp\left[-5.33(0.433 - \log r_{80})^2\right] \\ -4.7 \ln r_{80}\left[1 + \Theta r_{80}\right]^{-0.017 r_{80}^{-1.44}} \end{pmatrix}, \quad (10.18 \le U_{10}(m/s) \le 23.09) \tag{15b}$$

where Θ is an adjustable parameter, typically assigned the value 30 [*Gong*, 2003]. The Gong-Monahan parameterization (GM) was chosen because it explicitly incorporates the whitecap decay timescale as determined in the laboratory experiments of *Monahan et al*. [1982]. Additionally, GM and a version of GM modified to include the effects of sea surface temperature [*Jaeglé et al*., 2011] are widely used in 3-D chemical transport models such as GLOMAP (http://researchpages.net/glomap/) and GEOS-Chem (http://geos-chem.org/) [e.g., *Spracklen et al*., 2005; *Korohonen et al*., 2010; *Gantt et al*., 2012]. It is straightforward to substitute in place of 3.53 s in GM, the value of τ_{DWM} determined from the oceanic data in this study (5.3 s). Other whitecap timescales may be used by evaluating τ_{DWM} for a given data set. In contrast to the DWM, other variants of the whitecap method, such as the surf zone method, do not explicitly use a whitecap timescale. Many whitecap coverage parameterizations can be found in the literature, but *Callaghan et al*. [2008a] was chosen because it was determined for U_{10} up to ~23 m/s in the North East Atlantic Ocean, and each of the 109 values of W were measured from between 100 and 782 individual images, thereby lowering the statistical uncertainty associated with each W value [*Callaghan and White*, 2009]. Equations (15a) and (15b) can be divided by the whitecap coverage parameterizations of *Callaghan et al*. [2008a] and multiplied by a different parameterization to use a different whitecap scaling term. An obvious limitation of equations (15a) and (15b) is the use of a single value of τ_{DWM} for all wind speeds. As noted above, we have found τ_{DWM} to vary by a factor of 2.7 for the limited environmental and wave conditions considered here (see Table 1).

5.4. Integrated Sea-Salt Mass Flux

[28] Under the assumption that SSA particles are spherical and composed entirely of sea salt, the production flux in terms of the dry-particle radius (r_{dry}) can be integrated over

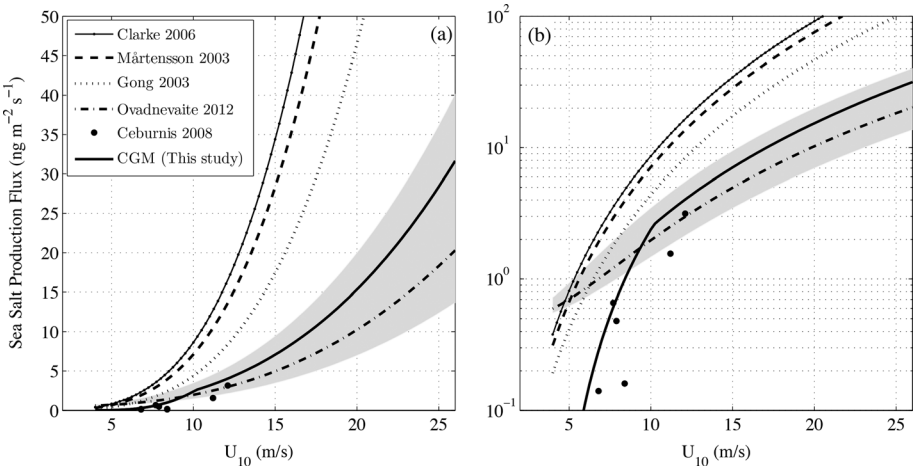

Figure 4. (a and b) Same data and parameterizations, but with a logarithmic *y*-axis in Figure 4b to highlight the data and parameterizations at low wind speeds. The shaded grey area is the range of uncertainty associated with the measurements of *Ovadnevaite et al*. [2012]. The filled black circles are from *Ceburnis et al*. [2008] as presented by *Ovadnevaite et al*. [2012]. Other parameterizations included for comparison are from *Clarke et al*. [2006] (thin dotted line), *Mårtensson et al*. [2003] (dashed line) and the Gong-Monahan model from *Gong* [2003] (dotted line). The thick solid black line is the integrated sea-salt mass flux calculated from equations (15a), (15b), and (16) and is termed CGM.

a size range ($r_{1,\mathrm{dry}}$ to $r_{2,\mathrm{dry}}$) and multiplied by the density of sea salt (ρ_{ss}) following

$$F = \frac{4}{3}\pi\rho_{\mathrm{ss}} \int_{r_{1,\mathrm{dry}}}^{r_{2,\mathrm{dry}}} \frac{\mathrm{d}F(r_{\mathrm{dry}})}{\mathrm{d}\log r_{\mathrm{dry}}} r_{\mathrm{dry}}^3 \mathrm{d}r_{\mathrm{dry}}, \qquad (16)$$

where $r_{\mathrm{dry}} \approx r_{80}/2$. *Ovadnevaite et al*. [2012] report high time-resolution measurements of the submicron ($0.029\,\mu\mathrm{m} < r_{80} < 0.580\,\mu\mathrm{m}$) SSA sea-salt mass concentration (mg m^{-3}) made over a 3 day period at wind speeds up to 26 m/s. They derive a sea-salt mass flux by multiplying the measured mass concentration measurements with estimates of the atmospheric boundary layer height and dividing by its filling time, τ_{bl}. Their results are shown in Figures 4a–4b (shaded grey area) as a function of wind speed where the vertical spread is associated with the range of reasonable values for τ_{bl}, (1 to 3 days were used). The wind speed parameterization from Ovadnevaite et al. (for which a value for τ_{bl} of 2 days was used) is also shown as the dash-dotted line [*Ovadnevaite et al*., 2012, their equation (2)]. Other field data shown are from *Ceburnis et al*. [2008], as presented by *Ovadnevaite et al*. [2012]. The sea-salt mass flux derived from equations (15a), (15b), and (16) is shown as the solid black line (hereafter referred to as CGM). The limits of integration for equation (16) were chosen to match the measurement range of *Ovadnevaite et al*. [2012] (i.e., $r_{1,\mathrm{dry}} = 1.45 \times 10^{-2}\,\mu\mathrm{m}$; $r_{2,\mathrm{dry}} = 2.9 \times 10^{-1}\,\mu\mathrm{m}$). It is important to note that the sea-salt mass flux calculated here is very sensitive to the upper integration cut-off value of $r_{2,\mathrm{dry}}$.

[29] Also shown for comparison are the predicted sea-salt mass fluxes following *Clarke et al*. [2006] and *Mårtensson et al*. [2003] (evaluated at a water temperature of 13°C) integrated over the same particle size range as above. The Clarke et al. and the Mårtensson et al. studies determined the number of SSA particles produced per whitecap area per unit time in the surf zone and in the laboratory, respectively, and scaled their results using the widely used whitecap coverage parameterization of *Monahan and O'Muircheartaigh* [1980]. Due to the methodology employed in these studies, the resulting parameterizations did not explicitly require the use of a whitecap timescale as used in the DWM. Consequently, the effect of varying whitecap timescale cannot be explicitly explored with these parameterizations. We note, however, that these parameterizations could be scaled to oceanic conditions using different whitecap coverage parameterizations. For example, whitecap parameterizations from *Lafon et al*. [2004, 2007], *Sugihara et al*. [2007] and *Callaghan et al*. [2008a, 2008b] would tend to yield lower sea-salt mass flux estimates as they predict lower estimates of whitecap coverage with wind speed than *Monahan and O'Muircheartaigh* [1980]. It is beyond the scope of this study to systematically evaluate the effects of whitecap coverage parameterization choice on SSA production flux parameterizations.

[30] The sea-salt mass flux estimate from CGM falls within the uncertainty range of *Ovadnevaite et al*., [2012] above 10 m/s. At this wind speed, the predicted mass flux from CGM is equivalent to using a τ_{bl} value of about 1.33 days, which lies within the 1–3 day range suggested by *Ovadnevaite et al*. [2012]. Between 8 and 10 m/s, the CGM parameterization agrees well with the data from *Ovadnevaite et al*. [2012] and *Ceburnis et al*. [2008]. At lower wind speeds, CGM follows the data of Ceburnis et al. more closely. We note that differences in the CGM sea-salt mass flux parameterization and any parameterization derived from in situ data sets would be sensitive to the presence of any background sea-salt mass concentrations not accounted for by CGM, and that these differences would be more evident at low wind speeds. The divergence between the two in situ data sets may represent differences in the magnitude of the source of the SSA particles, i.e., the nature and magnitude of wave breaking and whitecapping. It has been reported that the presence of swell waves can result in lower values of *W* at a given wind speed [e.g., *Sugihara et al*., 2007; *Callaghan et al*., 2008b; *Goddijn-Murphy et al*., 2011], and it may be reasonable to

assume then that the swell effect could be more pronounced at lower wind speeds when the ratio of swell to wind-wave energy may be largest.

6. Discussion

[31] Following a reevaluation of the discrete whitecap method, it is evident that the appropriate DWM whitecap timescale (τ_{DWM}) should be calculated as the area-weighted mean whitecap lifetime which includes both whitecap formation and decay timescales. This differs from the originally suggested whitecap decay timescale as it recognizes the contribution to whitecap lifetime from the whitecap formation phase and that whitecap lifetimes are not constant.

[32] An important result of the derived equation (13) above is that for a given value of $dE/d\log r_{80}$, which is assumed to be independent of τ_{DWM}, the SSA production flux determined with the DWM can vary at a given value of W (the assumption of independence between $dE/d\log r_{80}$ and τ_{DWM} is explored later in the discussion). For example, for a fixed value of W, if the area-weighted mean whitecap lifetime decreases, the breaking rate or characteristic maximum whitecap area would have to increase to maintain constant W (it may be less likely for the characteristic maximum whitecap area to increase to compensate for the decrease in whitecap lifetime since *Callaghan et al.* [2012] report a positive correlation between maximum whitecap size and whitecap decay time). Thus, from equation (13), it can be seen that an increase in breaking rate or characteristic maximum whitecap area would effectively result in a higher SSA production flux ($dF/d\log r_{80}$) for the fixed value of W (recall that when using constant $dE/d\log r_{80}$, any increase in $\tilde{A}_o$ results in a commensurate increase in $\Delta\tilde{n}$). Alternatively, the SSA production flux would increase with increasing whitecap coverage if the increases in W were caused by an increase in the breaking rate (R), or less likely $\tilde{A}_o$, since maximum whitecap area has been found to positively correlate with whitecap decay time as mentioned above. In practice, however, the possibility of variable SSA production flux at a given value of W is not realized with DWM SSA production flux models since a constant whitecap timescale is typically used and W is parameterized in terms of wind speed and not determined from its constituent terms as given by equation (11). Wave breaking rates, whitecap area distributions and lifetimes are rarely reported with measurements of W.

[33] The importance of using the correct value of τ_{DWM} has significant implications for SSA production flux modeling with the DWM. Essentially, whitecap coverage for a given observation period is a function of the wave breaking rate, the scale of the breaking waves and the lifetime of the whitecaps from formation to decay. All these details are encompassed in equations (8)–(11) above. Values of W, whether parameterized or measured directly, are therefore implicitly a function of τ_{DWM}. With the use of constant $dE/d\log r_{80}$ in the DWM, the SSA production flux is directly linked to the wave breaking rate and the scale of the breaking waves because τ_{DWM} appears in the denominator of the DWM (equation (4) above), as well as contributing to W. Therefore, the value of τ_{DWM} is important insofar as its value must correctly balance the role whitecap lifetimes play in governing the value of W. If not, then DWM-derived SSA production flux estimates will be biased high when τ_{DWM} is underestimated and biased low when τ_{DWM} is overestimated. Here, it has been shown that τ_{DWM} varied by up to a factor of 2.7 for this limited data set, but a single value of τ_{DWM} is used in the CGM SSA production flux parameterization (equations (15a), (15b)). Clearly, this value of τ_{DWM} cannot be expected to hold for all conditions and locations so that unknown systematic biases in DWM-derived estimates of the SSA production flux are likely to occur as a result of factors that result in variable whitecap lifetimes. Some of these controlling factors are discussed below.

[34] There are at least two regimes that influence variations in whitecap lifetimes: (i) surfactant stabilization of surface whitecap foam and (ii) variations in wave breaking scale and slope that drive variations in bubble plume characteristics which directly affect the surface whitecap lifetime [*Callaghan et al.*, 2013]. The decay of whitecap surface area is a strong function of the subsurface degassing bubble plume and hence the flux of bubbles to the surface whitecap, as noted before by *Monahan and Lu* [1990] and *Melville et al.* [2002]. This regime of whitecap decay is relevant whether or not stabilizing surfactants are present in the water column. In other words, when surfactants are absent or present in sufficiently low concentrations, the surface whitecap is present only as long as there is a bubble flux to the surface. It is important to note that smaller bubbles arrive at the sea surface that do not scatter sufficient light to form any discernible whitecap foam as detectable by most whitecap observation techniques. It is beyond the scope of this study to define this critical bubble size and concentration.

[35] Wave breaking dissipates wave energy which helps generate surface currents and creates turbulence [*Melville*, 1996]. Depending on the severity of breaking, breaking waves can be described as gently spilling (less energetic) or strongly plunging (more energetic). Indeed, *Monahan et al.* [1986] noted that aerosol productivity from gently spilling breaking waves and plunging breaking waves should be determined separately. Physical processes that affect the slope, scale, and intensity of breaking waves are likely related to many factors including the scale and development of the wave spectrum, the wave age, the portion of the wave spectrum that is breaking, the breaking rate, the presence or absence of nonlocally generated swell waves, wave-wave interactions, wave-current interactions, and the wind stress. For a given value of wind speed (U_{10}), it may be expected that all of the factors listed above can vary, leading to a wide variety of complex wave breaking patterns, subsurface bubble plumes and hence to variations in the bubble flux per whitecap area—something that has been shown to be an important quantity influencing the SSA production flux [*Mårtensson et al.*, 2003; *Keene et al.*, 2007; *Tyree et al.*, 2007].

[36] When stabilizing surfactants are present in high enough concentrations, the decay time is controlled by water chemistry in addition to the degassing bubble plume. In this regime, surfactant-stabilized whitecap foam can be present after the bubble plume has degassed, and there is no longer a flux of bubbles replenishing the surface whitecap. Bubble persistence on timescales longer than a few milliseconds is a consequence of gradients in the concentration of surfactants within the thin wall of a bubble or foam cell which in turn gives rise to surface tension gradients that cause "Marangoni" forces to retard gravity-driven fluid drainage from the thin film. Surfactants lower the surface tension of water by an amount

which can be quantified in terms of the film pressure, ξ. The film pressure is defined as the difference in surface tension between clean surfactant-free water and water with surfactant. Clean seawater has a nominal surface tension of 74 mN m^{-1} and oceanic film pressures have been measured in the range 1–23 mN m^{-1} [e.g., *Barger et al*., 1974]. The surface tension of clean freshwater decreases from about 74.9 mN m^{-1} to 71.2 mN m^{-1} as water temperature increases from 5°C to 30°C. Several studies have shown that a wide range of surfactants stabilize bubbles and foam, which extends their lifetime by seconds to minutes [e.g., *Garrett*, 1967b; *Ternes and Berg*, 1984; *Modini et al*., 2013; *Callaghan et al*., 2013]. Within the context of their effect on lifetimes of bubbles and foam in the oceanographic literature, surfactants have often been referred to as "insoluble" and "soluble." Insoluble surfactants have been shown to form monomolecular layers at air-water surfaces and while they always act to stabilize the thin fluid films somewhat, the increase in lifetime with increasing concentration is not monotonic, and there can be a peak in the lifetime to film pressure relationship [*Garrett*, 1967b; *Ternes and Berg*, 1984]. Laboratory experiments have shown that the "soluble" surfactant Triton-X 100 used in concentrations equivalent to conditions of medium ocean productivity [*Wurl et al*., 2011] can extend whitecap decay times by a factor of 3 to 4 for relevant oceanic film pressures of about 4 mN m^{-1} [*Callaghan et al*., 2013].

[37] The differences in decay times between the four observation periods in this study could reflect some combination of variations in the physical processes that control wave breaking intensity and variations in water chemistry that control bubble and foam stability. For example, the relatively low decay times in observational period III may reflect a predominance of gently spilling breaking waves as opposed to stronger, plunging type breakers. Additionally, processes such as competitive adsorption can change the vertical concentration and type of surfactants within the surface microlayer (upper mm of the water column [*Liss and Duce*, 1997]), thereby affecting thin film stability and foam lifetime (for further discussion, see *Callaghan et al*. [2012]).

[38] It is important to note a key difference between the DWM as developed by Monahan and colleagues, and other variants of the general whitecap method such as the continuous whitecap method (CWM). The CWM combines an estimate of the size-resolved number of SSA particles produced per unit whitecap area per second, $f_{wc}(r_{80})$, with an estimate of the whitecap coverage to predict the size-resolved interfacial number of SSA particles per unit ocean surface area per unit time [*Lewis and Schwartz*, 2004]. The term $f_{wc}(r_{80})$ has been determined experimentally using several types of steady state whitecaps generated by diffusing air through sintered glass frits or through steady state waterfalls [e.g., *Cipriano and Blanchard*, 1981; *Mårtensson et al*., 2003; *Keene et al*., 2007; *Tyree et al*., 2007]. However, as originally formulated by Monahan and colleagues, the goal of the DWM was not to determine the number of SSA particles produced per unit whitecap area per second. Rather, as described in the introduction above, the goal was to determine the number of SSA particles produced per unit whitecap area, $dE/d\log r_{80}$, from a laboratory simulated breaking wave over the entire lifetime of the resulting whitecap and associated degassing bubble plume. Then, assuming that the rate of production and the rate of decay of whitecap area per unit area sea surface were equal in conditions of steady state whitecap coverage, the rate of production of whitecap area per unit sea surface area could be approximated by W/τ_{decay}, [*Monahan*, 1971]. The product of $dE/d\log r_{80}$ and W/τ_{decay} would then give the number of SSA particles produced per sea surface area per second. The whitecap decay timescale in the original DWM was not related to the timescale over which SSA particles are produced, but rather it is a fundamental property of the whitecaps generated by breaking waves. Using the DWM, the production of SSA particles per whitecap area ($dE/d\log r_{80}$) cannot be combined with the whitecap timescale to calculate the number of SSA particles produced per whitecap area per unit time, $f_{wc}(r_{80})$, because $dE/d\log r_{80}$ includes SSA particles generated by rising bursting bubbles that do not scatter sufficient light to form discernible whitecap foam. In this regard, the DWM differs fundamentally from other variants of the whitecap method such as the continuous whitecap method.

[39] As currently implemented, the DWM assumes that $dE/d\log r_{80}$ is independent of whitecap lifetime. This seems unlikely since whitecap decay times, which typically made up 50% or more of whitecap lifetimes for this data set, are strongly governed by both bubble plume characteristics and water chemistry. The laboratory study of Callaghan *et al*. [2013, see their Figure 10] shows that for a given whitecap area, the whitecap decay time can vary by a factor of about 2 due to a larger volume of air entrained per unit surface whitecap area by more energetic breaking waves when surfactant stabilization of whitecap foam is minimized. It may then be reasonable to suggest that $dE/d\log r_{80}$ could also vary, echoing the laboratory findings that $f_{wc}(r_{80})$ is proportional to bubble volume flux for a given whitecap area. Any correlation between $dE/d\log r_{80}$ and whitecap lifetimes would have important implications for the DWM, and could provide a way of implementing a variable $dE/d\log r_{80}$ in DWM models. For a whitecap of given maximum area, the presence of surfactants can extend whitecap decay times by a further factor of 2 or more [*Callaghan et al*., 2013]. Several studies have noted that aerosol productivity can both increase and decrease in the presence of surfactants [e.g., *Blanchard*, 1963; *Paterson and Spillane*, 1969; *Garrett*, 1968; *Tyree et al*., 2007; *Modini et al*., 2013]. This highlights the importance of knowing the regime controlling oceanic whitecap decay times, and hence lifetimes, for the purposes of accurate SSA production flux modeling with the DWM or any method.

[40] The influence of water temperature on aerosol productivity has also been documented [e.g., *Woolf et al*., 1987; *Bowyer et al*., 1990; *Mårtensson et al*., 2003], although the effect of water temperature on whitecap lifetimes has not yet been thoroughly studied. Aerosol productivity has also been shown to be dependent on the degree of gas saturation in surface waters [e.g., *Stramska et al*., 1990]. Given that the formation and decay phases of whitecap area evolve differently due to different dominant physical processes, the number and size of aerosol produced as the whitecap evolves is also likely to change [e.g., *Woolf et al*., 1987], so that the ratio of formation to decay timescales, ψ, may also be an important factor when considering possible variations in $dE/d\log r_{80}$. Although the effects of water temperature on the SSA production flux with the DWM have now begun to be incorporated into the DWM [e.g., *Jaeglé et al*., 2011], the effects of variable whitecap lifetimes and aerosol productivity due to variations in water chemistry and bubble plume characteristics remain unaccounted for.

[41] Notwithstanding the limitations of the DWM as discussed above, there is good overlap between the CGM SSA production flux model presented here and the in situ sea-salt mass flux measurements of *Ovadnevaite et al*., [2012]. But it is clear that using a single value of wind speed and characteristic whitecap lifetime cannot encompass the entire range of physical and chemical processes that affect W, and the production flux of SSA particles. The range of possible values for τ_{DWM} reported here attests to that. Indeed, many expressions exist for the whitecap coverage parameterization (W) (for a comprehensive list of W parameterizations, see *Anguelova and Webster* [2006]) as well as the number of SSA particles produced per whitecap area [see *Lewis and Schwartz*, 2004]. Therefore, it must be stated that the overlap between the SSA production flux model presented here and the *Ovadnevaite et al*. [2012] data in Figure 4 may simply be fortuitous. Further observations of whitecap lifetimes in several locations by different investigators, coupled with appropriate detailed in situ measurements of bubble plume characteristics and surfactants are needed to fully understand the cause of variability in oceanic whitecap lifetimes. It is likely that advances in our understanding of the causes of oceanic whitecap lifetime variability, along with changes in wave breaking rate and whitecap scales, will provide valuable information pertinent to variability in both whitecap coverage and SSA production flux parameterizations and measurements.

7. Conclusions and Suggestions for Further Work

[42] The formation times of 552 oceanic whitecaps, as well as their entire lifetimes, have been presented. The two dimensional surface-evolution of the whitecaps measured here was found to be well-characterized by a nearly linear increase in area to a maximum value (A_o) (Figure 2), followed by a nearly exponential decrease in area with time. On a whitecap-by-whitecap basis, the ratio of the formation timescale to decay timescale (ψ) ranged from 0.1 to 0.7 for ~90% of the entire data set, with a distinctive peak between 0.2–0.3. The ratio was larger for observation period III, which had the shortest decay times and peaked at about $\psi \approx 0.5$–0.6. The data indicate that for the majority of whitecaps measured here, the formation time contributed 20% to 25% of the total whitecap lifetime, but could be as large as 70% or more. This represents a large fraction of the total whitecap lifetime especially in conditions where the formation time and decay time are of the same order, such as observation period III of the current data set. Whereas the formation times presented here exhibited similar distributions for all time periods, the corresponding decay times presented in *Callaghan et al*. [2012] did not. This implies that variability in whitecap lifetime within and between observation periods was largely driven by variability in processes controlling whitecap decay.

[43] The discrete whitecap method is a relatively straightforward and effective way to obtain estimates of the number of size-resolved SSA particles produced per unit sea surface area per unit time and as such is extensively employed in global aerosol microphysics models. Through a reexamination of its constituent terms, and by collecting a unique field data set of oceanic whitecap lifetimes, a revised whitecap timescale for this approach to parameterizing the SSA production flux is proposed. Key to this new DWM timescale (τ_{DWM}) was recognizing that whitecap lifetimes are variable and are the sum of their formation and decay times and defining an area-weighted mean whitecap lifetime to account for this natural variability. The value of τ_{DWM} for the entire data set was 5.3 s, but varied by a factor of 2.7 between 2.2 and 5.9 s across four different observation periods, importantly showing that τ_{DWM} should not be expected to remain constant between observation periods and most likely also between different geographical locations. The values of τ_{DWM} presented here should be considered lower bounds as the contributions from the largest whitecaps were not accounted for due to the limited camera field of view. From Table 1, no clear systematic dependence of $\tau_{wcap,eff}$ with wind speed over all periods is evident. However, when considering the only two contiguous time periods, i.e., periods III and IV, there was an increase in τ_{DWM} of almost a factor of 2 from 2.2 to 4.1 s over the course of about 1 h. During this time, the maximum 20 min average wind speed increased from 6.8 to 15.1 m/s (see row 8 in Table 1). Additionally, the minimum 20 min average wind speed from Period III of 4.2 m/s lies within the range of reported minimum wind speeds needed for the onset of visible whitecapping [e.g., *Monahan and O'Muircheartaigh*, 1986; *Callaghan et al*., 2008a]. This suggests that wind speed, in addition to a range of physical factors, likely played some role in the observed variation in τ_{DWM}. The importance of accurately knowing τ_{DWM} is pertinent to understanding variability in whitecap coverage and providing an estimate of the importance of wave breaking rate and whitecap scales to SSA production flux.

[44] Using a value of 5.3 s for τ_{DWM}, a new DWM SSA production flux parameterization was formulated by combining τ_{DWM} with available expressions for the number of SSA particles produced per unit whitecap area [*Gong*, 2003] and whitecap coverage [*Callaghan et al*., 2008a]. The parameterization was evaluated by calculating the integrated sea-salt mass flux ($1.45 \times 10^{-2} \leq r_{dry} \leq 2.9 \times 10^{-1}$ μm) for wind speeds up to 26 m/s and which were found to be within the range of uncertainty of the in situ measurements of *Ovadnevaite et al*. [2012]. While it has been noted that many existing SSA production flux parameterizations may overestimate sea-salt mass flux [*de Leeuw et al*., 2011], the formulation presented here predicts lower sea-salt mass fluxes than many previously published parameterizations.

[45] A limitation of the discrete and continuous whitecap methods as often implemented is that the number of SSA particles produced per whitecap area in the DWM, $dE/d\log r_{80}$, and the number of SSA particles produced per whitecap area per second in the CWM, $f_{wc}(r_{80})$, do not vary. It is noted that *Monahan et al*. [1986] suggested that $dE/d\log r_{80}$ should ultimately be determined separately for both spilling and plunging breaking waves. Several laboratory experiments have now shown that $f_{wc}(r_{80})$ is fundamentally linked to the bubble volume flux beneath the whitecap area [*Mårtensson et al*., 2003; *Keene et al*., 2007; *Tyree et al*., 2007]. Furthermore, this and other field studies have shown that whitecap decay times and lifetimes are not constant, and laboratory studies have shown that bubble plume characteristics fundamentally control the evolution of surface whitecaps in addition to influences from water chemistry [*Callaghan et al*., 2013]. A functional dependence between $dE/d\log r_{80}$ and whitecap lifetime is therefore possible, and studies investigating this relationship are warranted. This relationship would become more complex

in situations where surface water chemistry also significantly affects whitecap lifetime.

[46] With the goal of improving the DWM, careful evaluation of the variation of $dE/d\log r_{80}$ with different scales of breaking waves and water properties may be achieved in a laboratory setting recreating realistic breaking waves, bubble plumes, and whitecap foam. Several studies have shown that breaking waves and bubble size distributions realistic of the open ocean can be generated in the laboratory setting [e.g., *Deane and Stokes*, 2002; *Leifer and de Leeuw*, 2006; *Leifer et al*., 2006], and *Stokes et al*. [2013] and *Prather et al*. [2013] have suggested that recreating key features of breaking waves, such as the bubble size distribution and the intermittent nature of oceanic breaking waves, are essential features when trying to faithfully recreate realistic SSA particle size distributions and chemical complexity in the laboratory. Both approaches are able to recreate breaking waves and whitecaps of different scales in a controlled and repeatable manner in the laboratory in addition to varying physical, chemical, and biological properties of the water, with the added benefit of monitoring bubble size distributions, bubble plume timescales, and surface whitecap area and lifetime. As noted by *Lewis and Schwartz* [2004], laboratory studies can offer fruitful avenues with which to explore factors controlling SSA production flux.

[47] While laboratory studies are extremely useful as they allow for unprecedented control over experimental setup, they cannot replicate the full scale and complexity of the natural environment making field studies of SSA production indispensable. In terms of characterizing $dE/d\log r_{80}$ in the field, it is possible to measure all the terms that contribute to the instantaneous whitecap coverage such as the wave breaking rate, individual whitecap areas and lifetimes [e.g., *Kleiss and Melville*, 2011; *Callaghan et al*., 2012], and recently developed eddy correlation SSA measurement techniques [e.g., *Hill et al*., 2008; *Norris et al*., 2012, 2013] may provide a method to measure the in situ SSA production flux. In this way, the individual terms of equation (14) could be evaluated in the field in order to determine $dE/d\log r_{80}$ for a given set of environmental conditions. Further studies of whitecap coverage variability should strive to deconvolve the relative contributions of wave breaking rate, whitecap size distributions, and whitecap lifetimes to the overall value of W. While relatively straightforward to accomplish in the laboratory, an important and challenging aspect for field measurements of whitecap coverage will be to determine to what extent water chemistry affects whitecap lifetimes in addition to bubble plume characteristics.

[48] Finally, as currently implemented, the DWM does not explicitly separate the contribution to the SSA production flux from evolving whitecap foam and the contribution from the smaller bubbles that rise to the water surface in isolation in sufficient concentrations so as not to form any appreciable whitecap foam. A more detailed DWM incorporating production flux segmentation into the contribution from visible whitecap foam patches and the contribution from slowly rising isolated bubbles may yield an improved approach to SSA production flux modeling. Such an approach could incorporate models for the evolution of surface foam patches generated by realistic time-evolving bubble plume models. The foam models should strive to represent physical processes such as thin film fluid drainage rates [*Manev and Nguyen*, 2005], foam coarsening [e.g., *Saint-Jalmes and Langevin*, 2002] and the production of daughter bubbles from rupturing parent bubbles [*Bird et al*., 2010]. Since the number and size of SSA particles produced from a rupturing bubble is a strong function of bubble size, both foam coarsening and daughter bubble formation will likely play an important role in determining the distribution of SSA particles from an evolving whitecap foam patch and subsurface bubble population. Furthermore, upper ocean turbulence models would be useful in determining the rate at which bubbles rise to the surface, an important feature for the evolution of surface whitecaps and background bubble concentration. As wind speed increases, wind-driven oceanic turbulence increases trapping an increasing number of smaller bubbles within the upper few meters of the water column. *Deane et al*. [2013] show that bubbles of radius 200 μm and less can remain trapped in the upper few meters of the water column at wind speeds of 7 m/s. This trapping effect would effectively remove these bubbles as potential sources of SSA particles (e.g., jet drops) until such time as the water turbulence decreases or the bubbles dissolve in the water column. Such an effect may produce a steeper roll off in $dE/d\log r_{80}$ with increasing particle size as the wind speed increases, as well as producing a wind history hysteresis effect in SSA production flux.

[49] **Acknowledgments.** A.H.C. would like to thank Grant Deane and Dale Stokes for the collection of the sea surface images during the SPACE08 campaign which were used in this study. James Preisig of Woods Hole Oceanographic Institution is gratefully acknowledged for his considerable efforts running the SPACE08 campaign. A.H.C. would also like to thank J. Ovadnevaite for providing the aerosol size range measured by the aerosol mass spectrometer. The ideas discussed here were developed while A.H.C. was a visiting research fellow at the Deane laboratory at the Scripps Institution of Oceanography, and A.H.C. benefitted from valuable discussions with G. Deane. Writing of the paper began while A.H.C. was a member of Brian Ward's group at the National University of Ireland, Galway. A.H.C. was funded by the Irish Research Council and Marie Curie under FP7 and NSF grant OCE-1155123. The SPACE08 campaign was funded by the Office of Naval Research grants N00014-11-1-0158, N00014-10738, and N00014-11030. Comments from E. Lewis and G. Deane on an early version of the paper are greatly appreciated. The comments of E. C. Monahan and anonymous reviewers helped to greatly improve the paper.

References

Anguelova, M. D., and F. Webster (2006), Whitecap coverage from satellite measurements: A first step towards modeling the variability of oceanic whitecaps, *J. Geophys. Res.*, *111*, C03017, doi:10.1029/2005JC003158.

Barger, W. R., W. H. Daniel, and W. D. Garrett (1974), Surface chemical properties of banded sea slicks, *Deep-Sea Res.*, *21*, 83–89.

Bird, J. C., R. de Ruiter, L. Courbin, and H. A. Stone (2010), Daughter bubble cascades produced by folding of ruptured thin films, *Nature*, *465*, doi:10.1038/nature09069.

Blanchard, D. C. (1963), The electrification of the atmosphere by particles from bubbles in the sea, *Progr. Oceanogr.*, *1*, 73–202.

Bowyer, P. A., D. K. Woolf, and E. C. Monahan (1990), Temperature dependence of the charge and aerosol production associated with a breaking wave in a whitecap simulation tank, *J. Geophys. Res.*, *95*(C4), 5313–5319.

Callaghan, A. H., and M. White (2009), Automated processing of sea surface images for the determination of whitecap coverage, *J. Atmos. Oceanic Technol.*, *26*, 383–394.

Callaghan, A. H., G. Deane, and M. D. Stokes (2008a), Observed physical and environmental causes of scatter in whitecap coverage values in a fetch limited coastal zone, *J. Geophys. Res.*, *113*, C05022, doi:10.1029/2007JC004453.

Callaghan, A. H., G. de Leeuw, L. H. Cohen, and C. D. O'Dowd (2008b), The relationship of oceanic whitecap coverage to wind speed and wind history, *Geophys. Res. Letts.*, *35*, L23609, doi:10.1029/2008GL036165.

Callaghan, A. H., G. B. Deane, M. D. Stokes, and B. Ward (2012), Observed variation in the decay time of oceanic whitecap foam, *J. Geophys. Res.*, *117*, C09015, doi:10.1029/2012JC008147.

Callaghan, A. H., G. B. Deane, and M. D. Stokes (2013), Two regimes of laboratory whitecap foam decay: Bubble plume controlled and surfactant stabilized, *J. Phys. Oceanogr.*, *43*, 1,114–1,126, doi:10.1175/JPO-D-12-0148.1.

Ceburnis, D., C. D. O'Dowd, G. S. Jennings, M. C. Facchini, L. Emblico, S. Decesari, S. Fuzzi, and J. Sakalys (2008), Marine aerosol chemistry gradients: Elucidating primary and secondary processes and fluxes, *Geophys. Res. Letts.*, *35*, L07804, doi:10.1029/2008GL033462.

Cipriano, R. J., and D. C. Blanchard (1981), Bubble and aerosol spectra produced by a laboratory 'breaking wave', *J. Geophys. Res.*, *86*(C9), 8085–8092.

Clarke, A. D., S. R. Owens, and J. Zhou (2006), An ultrafine sea-salt flux from breaking waves: Implications for cloud condensation nuclei in the remote marine atmosphere, *J. Geophys. Res.*, *111*, D06202, doi:10.1029/2005JD006565.

Deane, G. B. (1997), Sound generation and air entrainment by breaking waves in the surf zone, *J. Acoust. Soc. Am.*, *102*(5), 2671–2689.

Deane, G. B. (2013), Determining the bubble cap film thickness of bursting bubbles from their acoustic emissions, *J. Acoust. Soc. Am.*, *133*(2), EL69–EL75.

Deane, G. B., and M. D. Stokes (2002), Scale dependence of bubble creation mechanisms in breaking waves, *Nature*, *418*, 839–844.

Deane, G. B., J. C. Preisig, and A. C. Lavery (2013), The suspension of large bubbles near the sea surface by turbulence and their role in absorbing forward-scattered sound, *Oceanic Eng. IEEE J.*, *PP*(99), 1,10, doi:10.1109/JOE.2013.2257573.

Fan, L. S., and K. Tsuchiya (1990), Bubble wake dynamics in liquids and liquid-solid suspensions, *Butterworth-Heinemann Series in Chemical Engineering*, 363 pp.

Gantt, B., M. S. Johnson, N. Meskhidze, J. Sciare, J. Ovadnevaite, D. Ceburnis, and C. D. O'Dowd (2012), Model evaluation of marine primary organic aerosol emission schemes, *Atmos. Chem. Phys.*, *12*, 8553–8566, doi:10.5194/acp-12-8553-2012.

Garrett, W. D. (1967a), The organic chemical composition of the ocean surface, *Deep Sea Res.*, *14*, 221–227.

Garrett, W. D. (1967b), Stabilization of air bubbles at the air-sea interface by surface active material, *Deep Sea Res.*, *14*, 661–672.

Garrett, W. D. (1968), The influence of monomolecular surface films on the production of condensation nuclei from bubbled sea water, *J. Geophys. Res.*, *73*(16), 5145–5150.

Goddijn-Murphy, L., D. K. Woolf, and A. H. Callaghan (2011), Parameterizations and algorithms for oceanic whitecap coverage, *J. Phys. Oceanogr.*, *41*, 742–756.

Gong, S. L. (2003), A parameterization of sea-salt aerosol source function for sub- and super-micron particles, *Global Biogeochem. Cycles*, *17*(4), 1097, doi:10.1029/2003GB002079.

Henry, C. L. (2010), Bubbles, thin films and ion specificity, *Ph. D. Thesis*, The Australian National University, pp. 220.

Hill, M. K., B. J. Brooks, S. J. Norris, M. H. Smith, I. Brooks, G. Leeuw de, and J. J. N. Lingard (2008), A compact lightweight aerosol spectrometer probe (CLASP), *J. Atmos. Oceanic Technol.*, *25*, 1,996–2,006, doi:10.1175/2008JTECHA1051.1.

Jaeglé, L., P. K. Quinn, T. S. Bates, B. Alexander, and J.-T. Lin (2011), Global distribution of sea salt aerosols: New constraints from in situ and remote sensing observations, *Atmos. Chem. Phys.*, *11*, 3137–3157, doi:10.5194/acp-11-3137-2011.

Keene, W. C., et al. (2007), Chemical and physical characteristics of nascent aerosols produced by bursting bubbles at a model air-sea interface, *J. Geophys. Res.*, *112*, D21202, doi:10.1029/2007JD008464.

Kleiss, J. M., and W. K. Melville (2011), The analysis of sea surface imagery for whitecap kinematics, *J. Atmos. Oceanic Technol.*, *28*, 219–243, doi:10.1175/2010JTECHO744.1.

Korohonen, H., K. S. Carslaw, P. M. Forster, S. Mikkonen, N. D. Gordon, and H. Kokkola (2010), Aerosol climate feedback due to decadal increases in Southern Hemisphere wind speeds, *Geophys. Res. Letts.*, *37*, L02805, doi:10.1029/2009GL041320.

Lafon, C., J. Piazzola, P. Forget, O. Le Calve, and S. Despiau (2004), Analysis of the variations of the whitecap fraction as measured in a coastal zone, *Bound. Lay. Meteorol.*, *111*, 339–360, doi:10.1023/B:BOUN.0000016490.83880.63.

Lafon, C., J. Piazzola, P. Forget, and S. Despiau (2007), Whitecap coverage in coastal environment for steady and unsteady wave field conditions, *J. Mar. Syst.*, *66*, 38–46, doi:10.1016/j.jmarsys.2006.02.013.

Lamarre, E., and W. K. Melville (1991), Air entrainment and dissipation in breaking waves, *Nature*, *351*, 469–472.

de Leeuw, G., E. L. Andreas, M. D. Anguelova, C. W. Fairall, E. R. Lewis, C. O'Dowd, M. Schulz, and S. E. Schwartz (2011), Production flux of sea spray aerosol, *Rev. Geophys.*, *49*, RG2001, doi:10.1029/2010RG000349.

Leifer, I., and G. de Leeuw (2006), Bubbles generated from wind-steepened breaking waves: 1. Bubble plume bubbles, *J. Geophys. Res.*, *111*, C06020, doi:10.1029/2004JC002673.

Leifer, I., G. Caulliez, and G. de Leeuw (2006), Bubbles generated from wind steepened breaking waves: 2. Bubble plumes, bubbles and wave characteristics, *J. Geophys. Res.*, *111*, C06021, doi:10.1029/2004JC002676.

Lewis, E. R., and S. E. Schwartz (2004), Sea salt aerosol production: Mechanisms, methods, measurements and models—A critical review, American Geophysical Union: Washington DC; Vol. Geophysical monograph 152.

Lippmann, T. C., and R. A. Holman (1989), Quantification of sand bar morphology: A video technique based on wave dissipation, *J. Geophys. Res.*, *94*(C1), 995–1,011.

Liss, P. S., and R. A. Duce (Eds.) (1997), *The Sea Surface and Global Change*, 519 pp., Cambridge Univ. Press, Cambridge, U. K., doi:10.1017/CBO9780511525025.

Manev, E. D., and A. V. Nguyen (2005), Critical thickness of microscopic thin liquid films, *Adv. Colloid Interface Sci.*, *114-115*, 133–146.

Mårtensson, E. M., E. D. Nilsson, G. de Leeuw, L. H. Cohen, and H. C. Hansson (2003), Laboratory simulations and parameterization of the primary marine aerosol production, *J. Geophys. Res.*, *108*(D9), 4297, doi:10.1029/2002JD002263.

Melville, W. K. (1996), The role of surface wave breaking in air-sea interaction, *Annu. Rev. Fluid Mech.*, *28*, 279–321.

Melville, W. K., F. Veron, and C. J. White (2002), The velocity field under breaking waves: Coherent structures and turbulence, *J. Fluid Mech.*, *454*, 203–233.

Meskhidze, N., et al. (2013), Production mechanisms, number concentration, size distribution, chemical composition, and optical properties of sea spray aerosols, *Atmos. Sci. Let.*, doi:10.1002/asl2.441.

Middleton, G. V. (2000), *Data analysis in the earth sciences using MATLAB*, Prentice Hall, New Jersey.

Modini, R. L., L. M. Russell, G. B. Deane, and M. D. Stokes (2013), Effect of soluble surfactant on bubble persistence and bubble-produced aerosol particles, *J. Geophys. Res. Atmos.*, *118*, 1,388–1,400, doi:10.1002/jgrd.50186.

Monahan, E. C. (1971), Oceanic whitecaps, *J. Phys. Oceanogr.*, *1*, 139–144.

Monahan, E. C., and M. Lu (1990), Acoustically relevant bubble assemblages and their dependence on meteorological parameters, *IEEE J. Oceanic Eng.*, *15*, 4.

Monahan, E. C., and I. O'Muircheartaigh (1980), Optimal power-law description of oceanic whitecap coverage dependence on wind-speed, *J. Phys. Oceanogr.*, *10*(12), 2,094–2,099, doi:10.1175/1520-0485.

Monahan, E. C., and I. O'Muircheartaigh (1986), Whitecaps and the passive remote sensing of the ocean surface, *Int. J. Remote Sens.*, *7*(5), 627–642, doi:10.1080/01431168608954716.

Monahan, E. C., and C. R. Zietlow (1969), Laboratory comparisons of fresh-water and salt-water whitecaps, *J. Geophys. Res.*, *74*(28), 6961–6966.

Monahan, E. C., K. L. Davidson, and D. E. Spiel (1982), Whitecap aerosol productivity deduced from simulation tank measurements, *J. Geophys. Res.*, *87*(C11), 8898–8904.

Monahan, E. C., D. E. Spiel, and K. L. Davidson (1986), A model of marine aerosol generation via whitecaps and wave disruption, in *Oceanic Whitecaps and Their Role in Air-Sea Exchange Processes*, edited by E. C. Monahan and G. MacNiochaill, pp. 167–174, Springer, New York.

Nolan, P. F. (1988), Decay characteristics of individual whitecaps, in *Oceanic Whitecaps and the Fluxes of Droplets From, Bubbles to, and Gases Through, the Sea Surface, Whitecap Rep. 4*, edited by E. C. Monahan et al., pp. 41–56, *Mar. Sci. Inst.*, Univ. of Conn., Groton.

Norris, S. J., I. M. Brooks, M. K. Hill, B. J. Brooks, M. H. Smith, and D. A. J. Sproson (2012), Eddy covariance measurements of the sea spray aerosol flux over the open ocean, *J. Geophys. Res.*, *117*, D07210, doi:10.1029/2011JD016549.

Norris, S. J., I. M. Brooks, B. I. Moat, M. J. Yelland, G. de Leeuw, R. W. Pascal, and B. Brooks (2013), Near-surface measurements of sea-spray production over whitecaps in the open ocean, *Ocean Sci.*, *9*, 133–145, doi:10.5194/os-9-133-2013.

O'Dowd, C. D., and G. de Leeuw (2007), Marine aerosol production: A review of current knowledge, *Phil. Trans. R. Soc. Acad.*, *365*, 1753–1774.

O'Dowd, C. D., M. C. Facchini, F. Cavalli, D. Ceburnis, M. Mircea, S. Decesari, S. Fuzzi, Y. J. Yoon, and J. P. Putaud (2004), Biogenically driven organic contribution to marine aerosol, *Nature*, *431*(7009), 676–680, doi:10.1038/nature02959.

Ovadnevaite, J., D. Ceburnis, M. Canagaratna, H. Berresheim, J. Bialek, G. Martucci, D. R. Worsnop, and C. O'Dowd (2012), On the effect of wind speed on submicron sea salt mass concentrations and source fluxes, *J. Geophys. Res.*, *117*, D16201, doi:10.1029/2011JD017379.

Paterson, M. P., and K. T. Spillane (1969), Surface films and the production of sea-salt aerosol, *Q. J. R. Meteorol. Soc.*, *95*(405), 526–534.

Prather, K. A., et al. (2013), Bringing the ocean into the laboratory to probe the chemical complexity of sea spray aerosol, *Proc. Natl. Acad. Sci. U. S. A.*, *110*(19), 7550–7555, doi:10.1073/pnas.1300262110.

Saint-Jalmes, A., and D. Lagevin (2002), Time evolution of aqueous foams: Drainage and coarsening, *J. Phys. Condens. Matter*, *14*, 9397–9412.

Scheludko, A. (1967), Thin liquid films, *Adv. Colloid Interface Sci.*, *1*, 391–464.
Sharkov, E. A. (2007), *Breaking Ocean Waves: Geometry, Structure and Remote Sensing*, Springer, Praxis Publishing Ltd, Chichester, UK.
Spracklen, D. V., K. J. Pringle, K. S. Carslaw, M. P. Chipperfield, and G. W. Mann (2005), A global off-line model of size-resolved aerosol microphysics: II. Identification of key uncertainties, *Atmos. Chem. Phys.*, *5*, 3233–3250.
Stokes, M. D., G. B. Deane, K. Prather, T. H. Bertram, M. J. Ruppel, O. S. Ryder, J. M. Brady, and D. Zhao (2013), A marine aerosol reference tank system as a breaking wave analogue for the production of foam and sea-spray aerosols, *Atmos. Meas. Technol.*, *6*, 1085–1094, doi:10.5194/amt-6-1085-2013.
Stramska, M., R. Marks, and E. C. Monahan (1990), Bubble-mediated aerosol production as a consequence of wave breaking in supersaturated (hyperoxic) seawater, *J. Geophys. Res.*, *95*(C10), 18,281–18,288.
Sugihara, Y., H. Tsumori, T. Ohga, H. Yoshioka, and S. Serizawa (2007), Variation of whitecap coverage with wave-field conditions, *J. Mar. Syst.*, *66*, 47–60.
Ternes, R. L., and J. C. Berg (1984), The effect of monolayer collapse on bubble stability, *J. Colloid Interface Sci.*, *98*, 471–477.
Tyree, C. A., V. M. Hellion, O. A. Alexandrova, and J. O. Allen (2007), Foam droplets generated from natural and artificial seawaters, *J. Geophys. Res.*, *112*, D12204, doi:10.1029/2006JD007729.
Woolf, D. K., P. A. Bowyer, and E. C. Monahan (1987), Discriminating between the film drops and jet drops produced by a simulated whitecap, *J. Geophys. Res.*, *92*(C5), 5,142–5,150.
Wurl, O., E. Wurl, L. Miller, K. Johnson, and S. Vagle (2011), Formation and distribution of sea-surface microlayers, *Biogeosciences*, *8*, 121–135, doi:10.5194/bg-8-121-2011.